Usefulness of Diffusion/Perfusion-weighted MRI in Rat Gliomas:

Correlation With Histopathology[1]

Guoguang Fan, PhD, MD, Peizhuo Zang, PhD, Fengdong Jing, MD, Zhenhua Wu, MD, Qiyong Guo, PhD, MD

Rationale and Objectives. Diffusion/perfusion-weighted MRI (DWI/PWI) can provide additional useful information in the diagnosis of patients with brain gliomas in a noninvasive fashion. However, the exact role of these new techniques is still undergoing evaluation. Our hypothesis was that DWI and PWI could be useful for assessment of growth and vascularity of implanted C6 rat gliomas.

Materials and Methods. Thirty-six rats were implanted with C6 glioma cells intracerebrally. Between 1 and 4 weeks after implantation, 8–10 rats were imaged on a clinical, 1.5-T whole-body magnetic resonance system with T_1-weighted imaging (T_1WI), T_2-weighted imaging, DWI, PWI, and postcontrast T_1WI at each weekly time point. All tumors were examined histologically; tumor cellularity and microvascular density were counted.

Results. On DWIs, statistical differences of apparent diffusion coefficient values for both the tumoral core and peritumoral region were present comparing tumors of 3–4 weeks' growth with tumors of 1–2 weeks' growth. Apparent diffusion coefficient value of tumoral core was negatively correlated with tumor cellularity ($r = -0.682$, $P < .01$). Statistical difference of maximal regional cerebral blood volume of tumoral core was present comparing 2–4 weeks with both 1 week after implantation and contralateral white matter ($P < .01$). Native vessel dilation in regions of normal brain at the periphery of the tumors at 1 week after implantation was observed. Correlation between maximal regional cerebral blood volume of tumor core and microvascular density was present ($r = 0.716$, $P < .01$).

Conclusion. DWI and PWI has potential to characterize C6 gliomas in rats, which is a promising model similar to human gliomas.

Key Words. C6 Gliomas; MR diffusion-weighted imaging; perfusion-weighted imaging; pathology.

Gliomas are the most common primary neoplasms of the brain, varying histologically from low grade to high grade. Even a single tumor mass may be histologically heterogeneous, representing a biologic continuum with varying degrees of cellular and nuclear pleomorphism, mitotic activity, vascular proliferation, and necrosis (1). Magnetic resonance imaging (MRI) is well-established modality for evaluating brain tumors. The use of gadolinium-based contrast agents yields further improvement in the demonstration and detection of cerebral gliomas. However, conventional postcontrast MRI does not provide any information regarding the tumor vascular beds of the brain because an increase in signal intensity reflects the accumulation of contrast agent in the interstitium of gliomas. Diffusion-weighted MRI (DWI), which is sensitive to the molecular diffusion of water, has been well established as a reliable noninvasive method for the early detection of cerebral ischemic stroke and has been reported to be helpful in differentiating necrotic cavities associated

Acad Radiol 2005; 12:640–651

[1] From the Department of Radiology, Second Hospital of China Medical University, Shenyang, China (G.F., F.J., Z.W., Q.G.); Department of Neurosurgery, First Hospital of China Medical University, Shenyang, China (P.Z.). Received December 16, 2004; revision requested January 26, 2004; revision accepted January 26, 2005. **Address correspondence to** G.F. e-mail: fanguog@vip.sina.com

doi:10.1016/j.acra.2005.01.024

with malignant gliomas from the benign ones (2). The use of diffusion-weighted imaging to better characterize enhancing tumors and vasogenic edema has been explored, but the results obtained have been conflicting (2,3) Only a few studies of DWI of peritumoral hyperintense regions seen on T_2-weighted MRIs have been performed (3). Therefore, the exact role of this new technique in the evaluation of intraaxial brain tumors is still undergoing evaluation. In fact, no obvious advantage of DWI is found with respect to the evaluation of tumor extension because the contrast between tumor and white matter is generally lower in DWI and apparent diffusion coefficient (ADC) maps as compared with conventional MRI (4).

Recent developments in perfusion-weighted MRI (PWI) techniques have permitted the creation of relative cerebral blood volume (rCBV) maps, leading to the qualitative and quantitative assessment of tumor vascularity. These maps have helped in the assessment of tumor grade and in targeting the site of biopsy (5). Although PWI has been widely used in brain tumor imaging, the exact relationship between imaging and pathologic findings has not been fully determined (5, 6). In part, this is because full quantitative correlation between PWI and histopathology requires a range of vascularity values that are difficult to obtain systematically in patients. In addition, it is not clear whether increases in PWI-derived rCBV measurements are due to the dilation of existing vessels or to an increase in total number of neocapillaries or both (7).

This study specifically addresses these issues by comparing MRI with histopathology in an established rat model of intracerebrally implanted C6 glioma cells. The C6 rat glioma cell line was originally isolated from an intracranial tumor in a rat exposed to N-nitroso-methylurea and is a reliable cell line model and yields good intracerebral growth, which permits a more uniform and predictable growth (8).

In this study, we have evaluated implanted C6 rat gliomas by MRI, DWI, and PWI to determine whether DWI measurements of ADC values were correlated with histologic assessments of tumor cellularity, and PWI measurements of rCBV were correlated with histologic assessments of microvascular density (MVD). Our hypothesis was that DWI and tumor ADC values could provide additional useful information in the assessment of gliomas, such as tumor malignancy and peritumoral infiltration; and PWI-derived rCBV measurements could be useful for the differentiation between dilation of existing host vessels and presence of neocapillaries, and thus provide quantitative validation of PWI methods used to assess the angiogenic status of human brain tumors.

MATERIALS AND METHODS

Rats and Tumor Implantation

Female Wistar rats, weighing 200–230 g were used for this study. All animal experimentation was conducted in accordance with the requirements and prior approval of the Institutional Animal Care and Use Committee at China Medical University.

The C6 rat glioma cells were kept frozen until use, then thawed and maintained in a monolayer culture in F12 medium with 10% calf serum. The rats were anesthetized with intraperitoneal injection of mixture of ketamine (50 mg/kg) and xylazine (4 mg/kg) and placed in a rodent stereotactic apparatus. Glial tumors were implanted into the left hemisphere by intracerebral injection of 1×10^5 C6 glioma cells in 5 μL 1.2% methylcellulose in F12 medium by a Hamilton syringe during 1- to 2-minute period. The coordinates used were 3 mm lateral and 1 mm anterior to the bregma, and 4.5 mm deep to the dural surface. As a control, five rats also received stereotactic injection of 5 μL phosphate-buffered saline without tumor cells in the same location in the contralateral cerebral hemisphere.

MRI Examination

A total of 41 rats, 36 with tumors and 5 healthy control animals without tumors, were included. Eight to ten different tumor-bearing rats were examined at each weekly time point between 1 and 4 weeks after the C6 cells implantation. After MRI, each rat was killed and every tumor was excised for histologic examination and comparison with MRI.

Contrast agent was injected through the tail vein, which was catheterized using a 1.0-mm diameter intravenous catheter. Successful puncture of the rat tail vein was controlled by blood reflux into the catheter and by injection of 0.9% NaCl. Gd-DTPA (Magnevist, Schering, Berlin, Germany) was used.

MRI examinations were performed on a clinical 1.5-T whole-body MRI system (GE Signa MR/i Hispeed Plus; GE Medical Systems, Milwaukee, WI). All images were acquired using a 3-cm internal diameter quadrature radiofrequency coil positioned over the rat head. Images were acquired parallel to the anteroposterior axis of the animal (axial). After scout view MRI, the examination protocol

consist of precontrast conventional MRI followed by DWI, PWI, and, finally, postcontrast T_1-weighted images.

Conventional MRI

Precontrast conventional MRI included axial T_1- and T_2-weighted MRIs (T_1-weighted spin-echo MRI: repetition time (TR) = 540 ms, echo time (TE) = 11.5 ms, one acquisition, field of view = 8 × 8 mm, matrix = 256 × 160, slice thickness = 2 mm, 16 slices, total imaging time = 2.5 minutes; T_2-weighted fast spin-echo MRI: TR = 4,900 ms, TE = 86 ms, one acquisition, field of view = 8 × 8 mm, matrix = 256 × 160, slice thickness = 2 mm, 16 slices, total imaging time = 4.5 minutes).

DWI

DWIs (b values = 0, 1000) were performed by using the echo-planar imaging sequence that combined the motion-probing gradient before and after the 180° pulse with echo-planar imaging readout, and fat was suppressed by placing a frequency-selective radiofrequency pulse before the pulse sequence. The parameters were: TR = 1000 ms, TE = 94.9 ms, slice thickness = 2 mm, intersection gap = 0, field of view = 8 × 4.8 mm, matrix = 96 × 128, bandwidth = 79 kHz, gradient strength = 22 mT, duration of diffusion gradients = 31 ms, and gradient separation = 42 ms in three orthogonal directions.

PWI

A single slice that best showed the tumor on T_2-weighted images was selected for PWI. A single shot echo-planar gradient echo sequence (TR = 24 ms, TE = 10 ms, flip angle, 10°, field of view = 8 × 8 mm, matrix = 64 × 64, slice thickness = 2 mm, intersection gap = 0) was used for PWI. After three images were obtained, an intravenously administered bolus of 0.1-mmol/kg Gd-DTPA (10× diluted in 0.9% NaCl) was administered by hand within 2 seconds into the tail vein. The imaging time was 2.8 seconds per image, with 42 consecutive images obtained. Finally, an additional set of contrast-enhanced T_1-weighted images was obtained using the same slice locations and slice thickness as PWIs.

MRI Analysis

The signal intensity of the solid portion of the tumor was visually assessed on precontrast conventional MRI. The enhancement patterns of tumors at different weekly time points were observed and the diameters of tumors were also assessed on both T_2-weighted images (T_2WI) and contrast-enhanced T_1-weighted images (T_1WI). Tumor enhancement was assessed by calculation of contrast-to-noise ratios of solid tumors from both precontrast and postcontrast T_1WI.

The ADC maps and values were calculated on a separate workstation (SUN, GE Adw3.1; GE Medical Systems, Milwaukee, WI). We recorded the ADC values from both the solid portion of the tumor (seen as the highest signal intensity lesion on DWI with a diffusion-weighting factor, b value of 1,000 seconds/mm^2 and with no diffusion gradient [ie, b = 0]) and peritumoral area (hyperintense on T_2WI, but not enhancing on postcontrast T_1WI). The ADC values in our study represented averaged ADCs of three to five regions of interest (ROIs). An ROI ranging in size from 8 to 20 mm^2 was drawn and positioned carefully to avoid contamination from adjacent different tissues. The ROI was drawn as large as possible using a circular or rectangular ROI on the workstation. As a control, the ADC was obtained from contralateral normal white matter.

Raw PWIs were transferred to a Unix workstation (SUN, GE Adw3.1) for postprocessing. Our technique depends on deconvolution with an arterial input function. Voxels that compose this arterial input function are manually selected by choosing voxels near the ipsilateral middle cerebral artery. For each voxel, the time-intensity curve for the dynamic images is converted first to a curve of change in T_2 and then of concentration versus time. Maps of rCBV were finally generated. The rCBV was determined by using a gamma-function fitting analysis of the first-pass concentration-time curve to avoid contamination from recirculation of the contrast agent. ROI analyses were performed on the solid portion of the tumor, on peritumoral area, and on the contralateral normal white matter, respectively. ROI was placed carefully to cover the region of maximum rCBV (areas of high perfusion on the CBV maps, mean area = 5.0 mm^2 ± 2.8). Additionally, we measured the ratio of rCBV in either the tumor or peritumoral area to that in the contralateral normal white matter to standardize variations in each examination.

Histologic and Immunochemical Examination

Immediately after MRI, all animals were sacrificed by an overdose of anesthetic. Brains were removed and placed in 4% paraformaldehyde with 30% sucrose at 4°C overnight. After the brains were fixed, they were embedded in paraffin, sectioned (5 μm), and stained with hema-

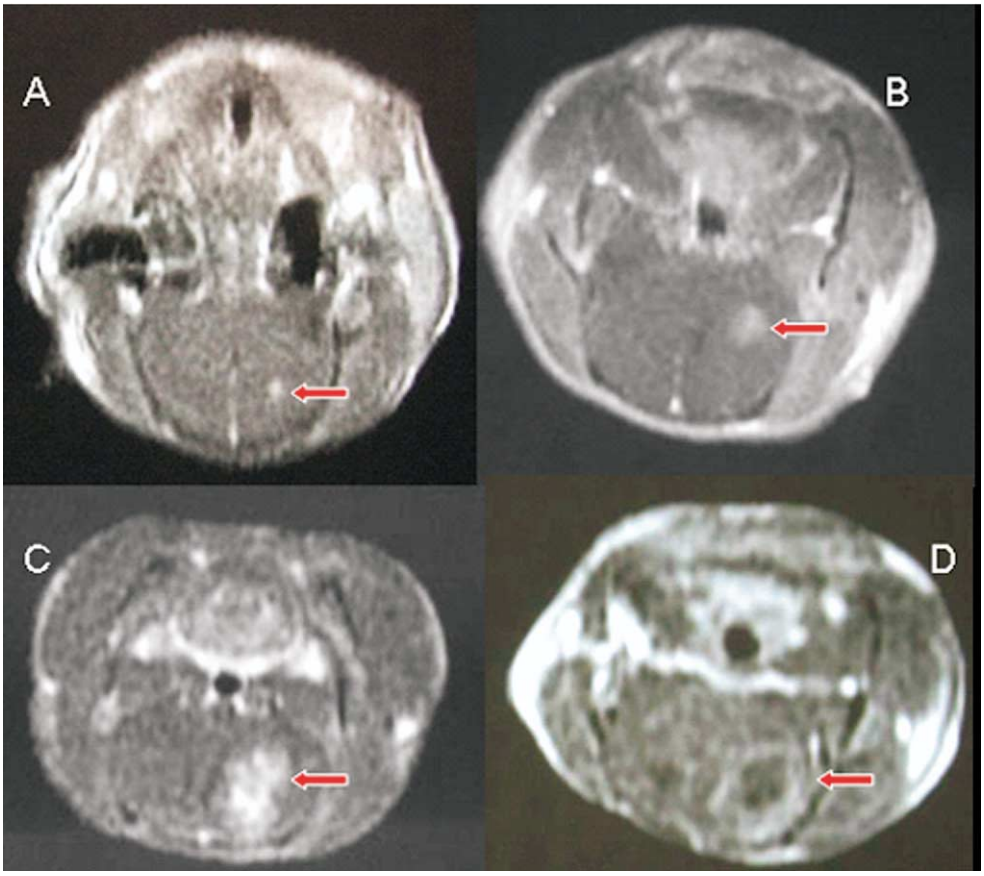

Figure 1. Magnetic resonance imaging (MRI) contrast-enhanced T_1-weighted images of C6 gliomas in different implantation period. **(a)** 1 week. **(b)** 2 weeks. **(c)** 3 weeks. **(d)** 4 weeks. MRI demonstrated the gradually increase in tumor size over the 4-week postimplantation period and central necrosis was present 4 weeks after the C6 cells implantation.

toxylin and eosin for conventional light microscopy using standard protocols.

All hematoxylin and eosin images were transferred to the separate workstation. Tumor cellularity, analyzed using an imaging software (Scion Image Beta 4.02 software for Windows; Scion Corp., Frederick, MD), was defined as the total area of nuclei of tumor cells divided by the area of the histologic section (original magnification ×400).

Immunohistochemical analysis with anti-CD34 stain was performed by using the avidin-biotin-peroxidase complex method to determine the vascularity of the tumors. MVD of tumorous tissue sections was evaluated according to Gasparini's criteria by one pathologist (H.S.) who was blinded with respect to the result of the MRI findings. At low power field (×100), the tissue sections were screened and 10 areas with the most intense neovascularization (hot spots) were selected. Microvessel counts of these areas were performed at high power field (×400). Any brown-stained endothelial cell or endothelial cell cluster that was clearly separated from adjacent microvessels, tumor cells, and connective elements was counted as one microvessel, irrespective of the presence of a vessel lumen. The mean microvessel number of the 10 most vascular areas of each tumor was taken as the MVD (9). To reduce observer-related variation, counting of the microvessels was performed with a computer image analyzer (MetaMorph Imaging System Version 6.2, Universal Imaging Corp., Downingtown, PA).

Statistical Analysis

All data obtained were summarized as the mean ± standard deviation (SD). Separate statistical comparisons of the tumor cellularity with the averaged ADC values of solid portion of tumor, and MVD with maximum relative rCBV were made using simple linear regression analysis. The Student's *t*-test was used to determine if there were statistically significant differences in both averaged ADC value and maximum relative rCBV among the implanted

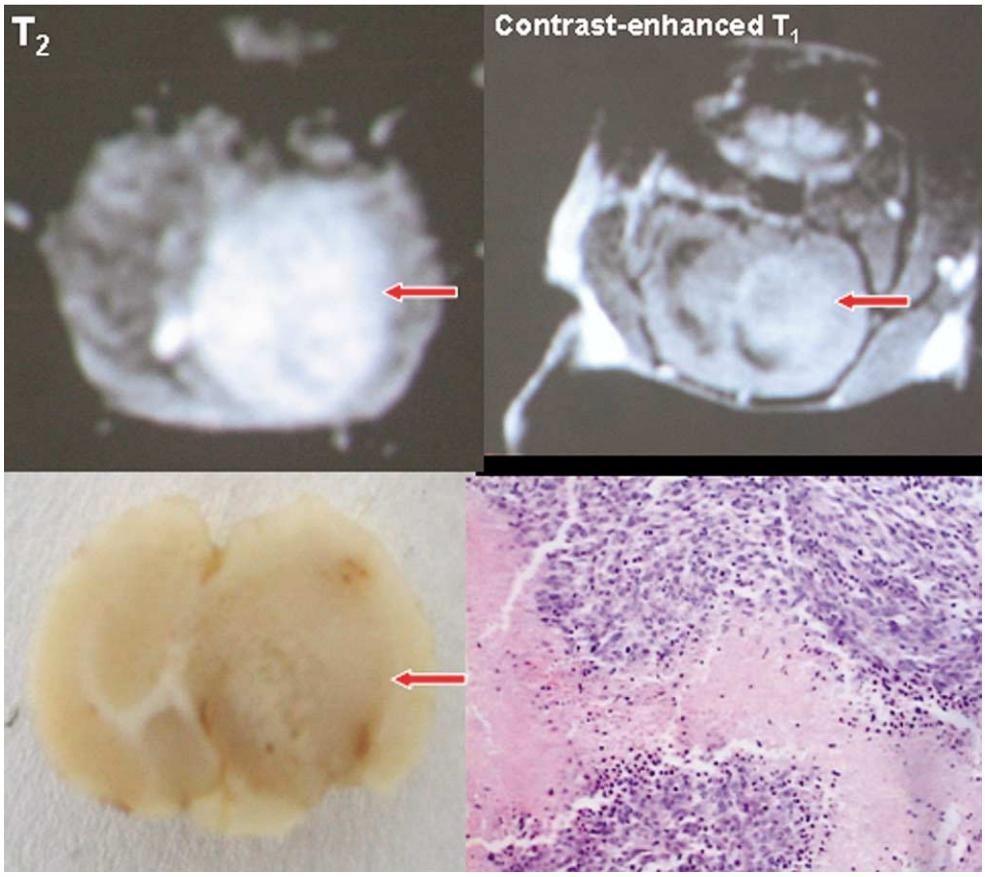

Figure 2. Magnetic resonance imaging of C6 gliomas 4 weeks after C6 cell implantation. **(a)** T_2-weighted images (T_2WI). **(b)** Contrast-enhanced T_1-weighted images (T_1WI). **(c)** Cross-section morphology. **(d)** Hematoxylin and eosin-stained image (×50). Tumor invasion area on T_2WI is greater than the area showed by contrast-enhanced T_1WI at later stages of tumor growth. There was extensive heterogeneity on both T_1WI and T_2WI, with irregular rim enhancement and clear evidence of central necrosis.

tumors at different weekly time points. A P value of less than .05 was considered to indicate statistical significance.

RESULTS

Conventional MRI Versus Histopathology

MRI demonstrated the gradually increase in tumor size over the 4-week postimplantation period (Fig. 1). All tumor tissues exhibited hyperintense on T_2WI and hypointense on T_1WI (Fig. 2), and all tumors exhibited enhancement after contrast administration. Both T_2WIs and contrast-enhanced T_1WIs enabled detection of small tumors with a diameter of less than 2 mm 1 week after tumor implantation. No significant change of tumor size on both T_2WI and contrast-enhanced T_1WI was observed between 1 week and 2 weeks after tumor implantation ($P > .05$); no change on contrast-enhanced T_1WI ($P > .05$), but difference on T_2WI was observed between 3 and 4 weeks ($P < .01$). However, significant change of tumor size on both T_2WI and contrast-enhanced T_1WI was present when tumors of 1–2 weeks' growth and tumors of 3–4 weeks' were compared ($P < .001$).

Rats were killed 1–4 weeks after tumor cells were implanted. All of the rats had grossly visible tumors averaging 7.33 ± 3.164 mm in diameter when the rats were killed and the rate of tumorigenesis was 100%. Histopathologic analysis showed that tumors were grown intracerebrally to form tumors with several characteristics of malignant glioma including nuclear pleomorphism, foci of tumor necrosis, intratumoral hemorrhage, and parenchymal invasion. Tumor extension was assessed by correlation of hematoxylin and eosin images with both T_2WI and contrast-enhanced T_1WI. Analysis of the brain adjacent to tumor shows that the actual tumor cell invasion area is greater than the area showed by contrast-enhanced T_1WI at later stages of tumor growth.

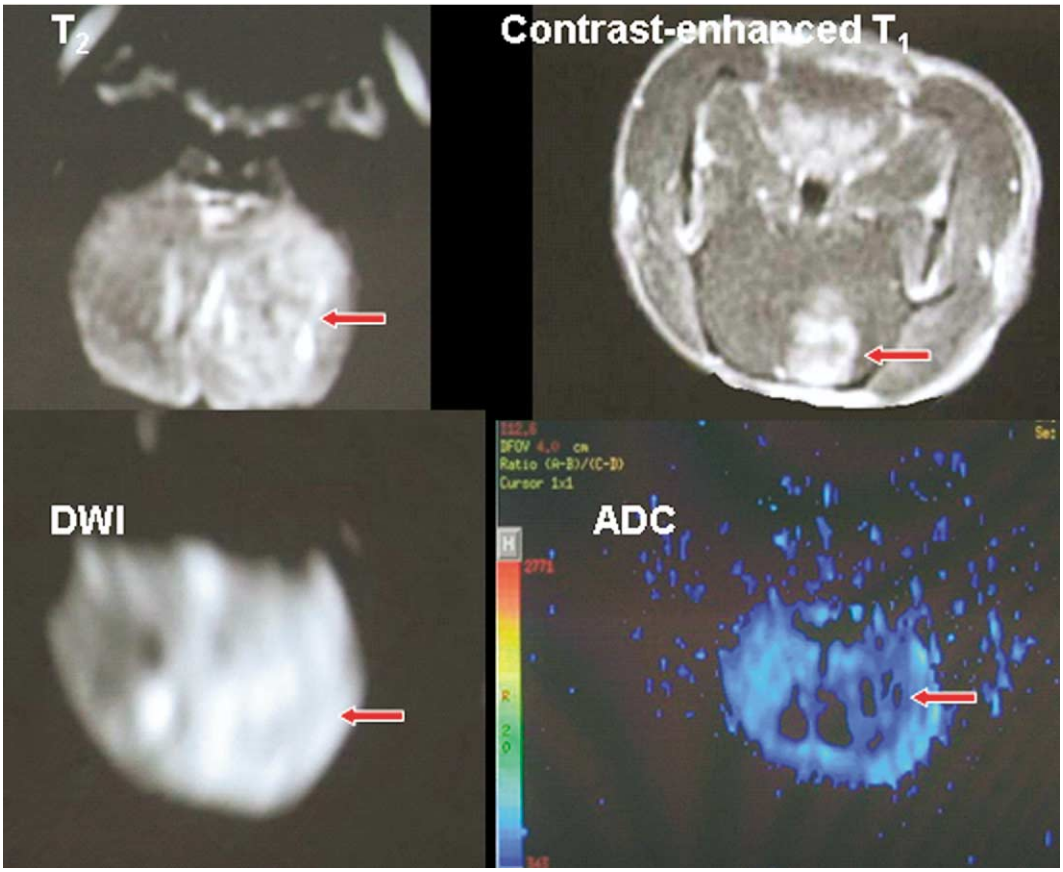

Figure 3. Magnetic resonance imaging (MRI) of C6 gliomas 3 weeks after C6 cell implantation. **(a)** T_2-weighted images. **(b)** Contrast-enhanced T_1-weighted images. **(c)** diffusion-weighted MRI (DWI). **(d)** Apparent diffusion coefficient (ADC) map. The signal intensity in the solid portion of the tumor was hyperintense on DWI (b = 1,000) and hypointense on ADC map with respect to the white matter.

DWI Versus Histopathology

On DWIs (b = 0, 1000), the signal intensity in the solid portion of the tumor was hyperintense with respect to the white matter (Fig. 3). The averaged ADC values for the solid tumor component ranged from 0.35 to 1.43 $\times$ 10^{-3} mm^2/second (mean, 0.891 $\pm$ 0.313 $\times$ 10^{-3} mm^2/second) and for white matter from 0.71 to 1.32 $\times 10^{-3}$ mm^2/second (mean 0.936 $\pm$ 0.171 $\times$ 10^{-3} mm^2/second).

The averaged ADC values of solid portion of tumor gradually fell over the 4-week postimplantation period (Table 1). No significant change of averaged ADC values in both the solid portion of tumor and the peritumoral area was observed within 3 weeks of tumor implantation ($P > .05$); in contrast, significant change was present only 4 weeks after tumor implantation ($P < .05$). In addition, significant change of averaged ADC values in both

Table 1
ADC Values Comparison of C6 Gliomas With Contralateral White Matter ($\times 10^{-3}$ mm^2/second)

Postimplantation	Cases	Solid Tumoral Region	Peritumoral Area	Contralateral White Matter
1 week	9	1.27 $\pm$ 0.14	1.15 $\pm$ 0.16	0.98 $\pm$ 0.16
2 weeks	10	0.97 $\pm$ 0.17	1.06 $\pm$ 0.18	0.97 $\pm$ 0.17
3 weeks	9	0.72 $\pm$ 0.10*	0.69 $\pm$ 0.13*	0.99 $\pm$ 0.14
4 weeks	8	0.52 $\pm$ 0.11*	0.79 $\pm$ 0.07*	1.00 $\pm$ 0.17

Data are mean $\pm$ standard deviation.
*Statistical significance ($P < .01$).

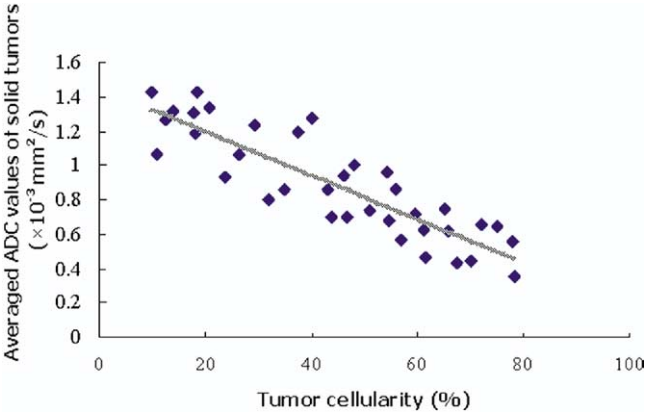

Figure 4. Tumor cellularity versus the apparent diffusion coefficient values of solid portion of C6 tumors. There is a negative correlation between them ($P = -.87$, simple regression analysis).

solid tumoral area and peritumoral area was present when tumors of 1–2 weeks' growth and tumors of 3–4 weeks' growth were compared ($P < .01$).

The relationship of tumor cellularity with the averaged ADC value of solid portion of tumor is showed in Fig. 4; the averaged ADC value correlated well with tumor cellularity ($r = -0.682$, $P < .01$).

PWI Versus Histopathology

The signal intensity of tumors was homogeneous on rCBV map within 2 weeks of tumor implantation. However, slight increases of signal intensity were observed in peritumoral area for nine cases of 1-week's growth tumors and six cases of 2-weeks' growth tumors (Fig. 5), suggesting dilated host blood vessels. In contrast, all rCBV maps for tumor of 3–4 weeks' growth were inhomogeneous, with various increases of the solid portion of tumor signal intensity (Fig. 6, Fig. 7).

Table 2 summarizes the measurements of maximum rCBV. Measured maximum rCBV in the solid portion of tumor varied from 0.56 to 10.65, with a mean of 3.92 ± 2.94 (±SD); whereas, in peritumoral area, maximum rCBV varied from 0.76 to 3.15, with a mean of 1.76 ± 0.83 (±SD). Measured values of maximum rCBV in the solid portion of tumor for the four groups (1–4 weeks) are plotted in Fig. 8. Statistically significant difference of measured values of maximum rCBV in the solid portion of tumor was present when 1 week's tumor growth and 2–4 weeks' growth tumors were compared ($P < .01$). Meanwhile, in early tumor stage (1–2 weeks), measured values of maximum rCBV in peritumoral area were elevated when compared with the contralateral white matter, making this difference statistically significant ($P < .05$).

Measured values of MVD of tumor for the four groups (1–4 weeks) are plotted in Fig. 9. Measured values of microvessel counts varied from 1.33 to 17.95, with a mean of 6.41 ± 4.56 (±SD). To determine whether maximum rCBV of solid portion of tumor was predictive of MVD, simple linear regression analysis was implemented (Fig. 10). The results indicated that maximum rCBV of tumor correlated well with MVD ($r = 0.724$, $P < .01$).

DISCUSSION

Numerous experiments in which the C6 rat glioma implantation model has been used have demonstrated characteristics consistent with human glioblastoma multiforme (10). Experimental glioma tumor model is promising for preclinical studies on human cerebral glioma; the feasibility to image these tumors was examined using morphologic, DWI, and PWI. These MRI methods also gain importance when investigating gliomas in patients.

Examination of rats by using conventional MRI provides numerous opportunities to develop our understanding of these malignant glial neoplasms. This study shows that these neoplasms can be followed with serial MRI, which allows for quantitative growth estimates in vivo. MRI demonstrated the gradually increase in tumor size over the 4-week postimplantation period. However, the tumor growth was nonproportional: the tumor grew relatively slowly in the early stage (1–2 weeks after tumor implantation), whereas it grew rapidly and became more infiltrative in late stages (3–4 weeks after tumor implantation). Signal characteristics of experimental tumors were similar to gliomas in humans: the tumor tissue exhibited typical hyperintense on T_2WI and hypointense on T_1WI. In the early stage of tumors (1–2 weeks; $n = 19$), the signal intensity of the tumor was homogeneously increased. The tumor margin appeared well demarcated from the adjacent normal brain and there was no evidence of central necrosis or peritumoral edema. In contrast, in late tumors (3–4 weeks; $n = 17$), there was extensive heterogeneity on both T_1WI and T_2WI, with irregular rim enhancement and clear evidence of central necrosis. Our results also showed that the diameters on T_2WI were more extensive than on contrast-enhanced T_1WI in the late stage of tumors. Comparison studies of MRI signal abnormality areas and histologic tumor areas also were performed. Analysis of the brain adjacent to tumor shows

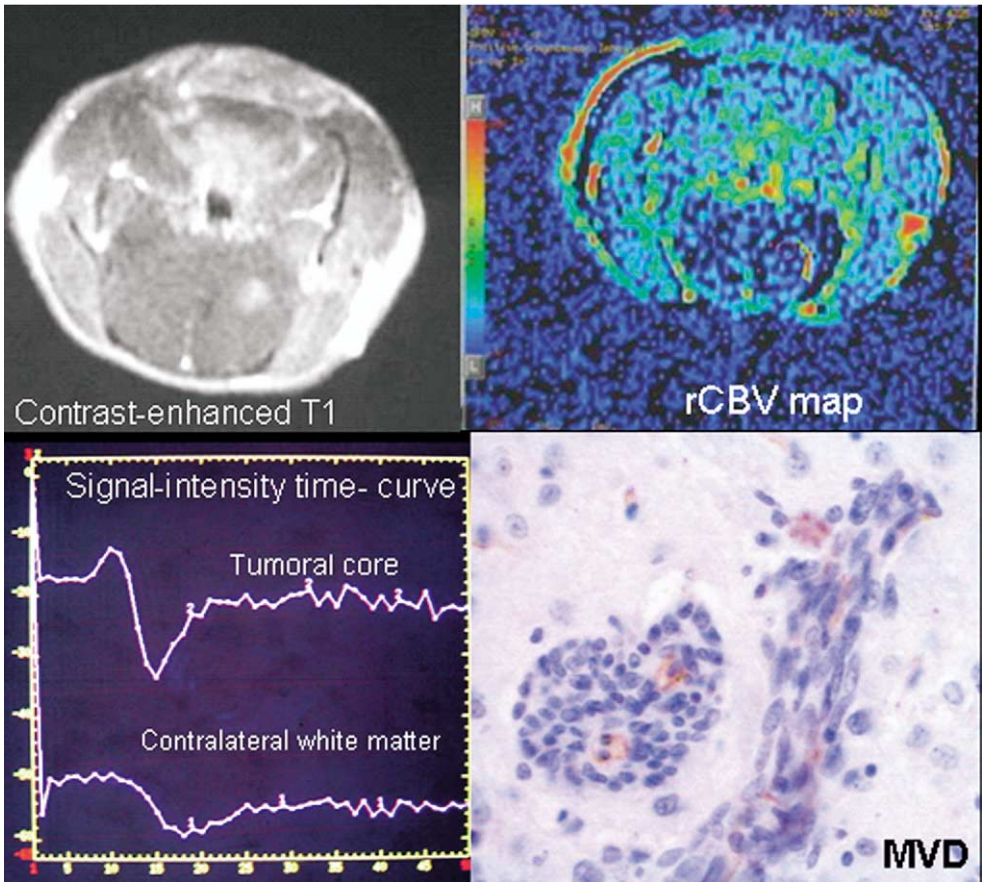

Figure 5. Perfusion-weighted magnetic resonance imaging of C6 gliomas 2 weeks after C6 cell implantation. **(a)** Contrast-enhanced T_1-weighted images. **(b)** Relative cerebral blood volume map. **(c)** Signal-intensity time curve. **(d)** Immunohistochemical image of CD34 (×400). A slight increase of signal intensity was observed in the peritumoral area, signal-intensity time curve fell slightly, and the immunohistochemical image of CD34 showed dilated host blood vessels.

that the actual tumor cell invasion area is greater than the area showed by contrast-enhanced T_1WI and slightly smaller than that by T_2WI in the late stages of tumor. Therefore, the true margin of a late-stage tumor is not defined only by the region of T_1 contrast enhancement; often, it is also not defined by the margin of T_2 signal abnormality because T_2 signal abnormality may reflect both infiltrating tumor and tumor-induced brain edema, and thus may overestimate the actual size of tumor. The true peritumoral region is commonly found in normal-appearing brain parenchyma at conventional imaging (11).

Diffusion-weighted MRI has been used by some to evaluate intra-axial tumors (12). Diffusion-weighted imaging and calculation of ADC values have been used to distinguish the normal white matter areas from necrosis, cyst formation, edema, and solid enhancing tumor. In the current study, DWI could improve the preoperative diagnostic effectiveness of MRI in patients with brain tumors, and calculated ADC values were statistically significant and useful in the grading of malignant tumors (13). Our result showed that calculated ADC values from tumoral core added more information to MRI in the differentiation and grading of different stage of tumor, these results support the use of ADC value in human brain tumors.

Contrary to previous findings, one of the major findings in our study was that averaged ADC values in peritumoral area were significantly different when early-stage and late-stage tumors were compared ($P < .01$). It is assumed that malignant gliomas are not strictly focal lesions, but rather are characterized by intracerebral dissemination of malignant glial cells along the myelinized axons and blood vessels or through the subarachnoid space (14). We postulate this may result in the difference of ADC values in peritumoral area; thus, we think that ADC value in peritumoral area is valuable for demarcation of glial original tumor though a partial volume effect con-

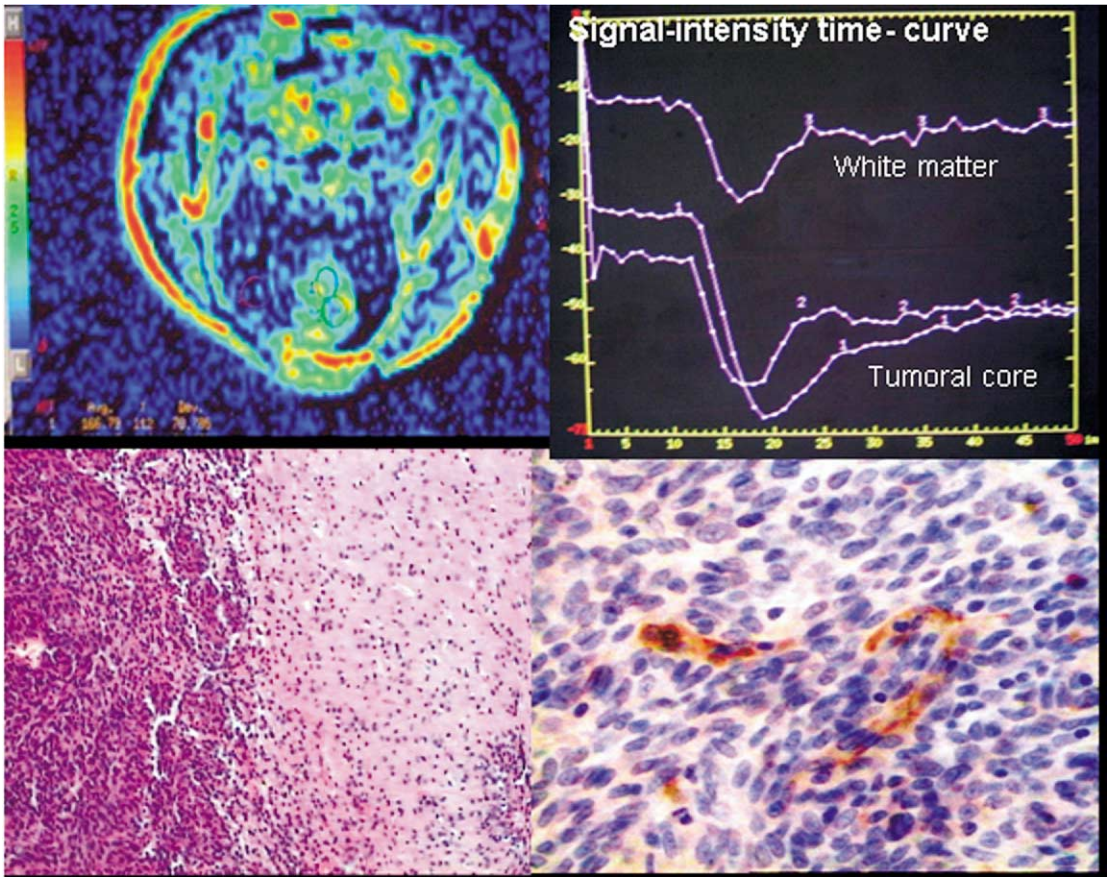

Figure 6. Perfusion-weighted magnetic resonance imaging of C6 gliomas 3 weeks after C6 cell implantation. **(a)** Contrast-enhanced T_1-weighted images. **(b)** Relative cerebral blood volume (rCBV) map. **(c)** Signal-intensity time-curve. **(d)**Immunohistochemical image of CD34 (×400). Measured values of maximum rCBV in the solid portion of tumor were increased; the signal-intensity time curve fell.

taminated by surrounding edema may affect the accurate outcome.

Our study also showed that the averaged ADC value from tumoral core correlated well with histologic cellularity. Tissue water diffusion is characterized by complexity. Its magnitude and direction depend on the permeability and spacing of diffusion barriers, as well as viscosity of the suspending medium (15). Characterization is also complicated by bulk flow within capillaries and by tissue water active transport processes. The protons in the brain included in the diffusion characterization are contained in water, whereas protons within macromolecules and membranes themselves make no contribution to this characterization because they are relatively immobile and have extremely short T_2 values (16). Therefore, the water diffusion in gliomas may be affected mainly by tumor cellularity, because the motion of water in the interstitium is the main contributor to increased ADC values. However, when visual inspection of the scatter of points for linear correlation between ADC value and cellularity was made, we also found that not all points fit very well, and there appear to be relatively few points above or below the line, which also deviate even further though the points plotted appear to scatter randomly either side of the line of best fit. Because statistical difference between ADC value and cellularity was assessed by one-way analysis of variance to correlate between two variables, these features in a scatter diagram suggest that there are many determinants except cellularity affecting ADC values in brain tissues, which needs further investigation using multivariate analysis.

New blood vessel growth is a critical phase of solid tumor growth. The growth of a solid tumor mass at 1–2 mm^3 depends on simple diffusion for oxygen, nutrients, and other essential materials. However, tumor mass growth larger than 1–2 mm^3 cannot grow and metastasize without angiogenesis (17). PWI techniques now have been used to assessment of tumor vascularity in vivo.

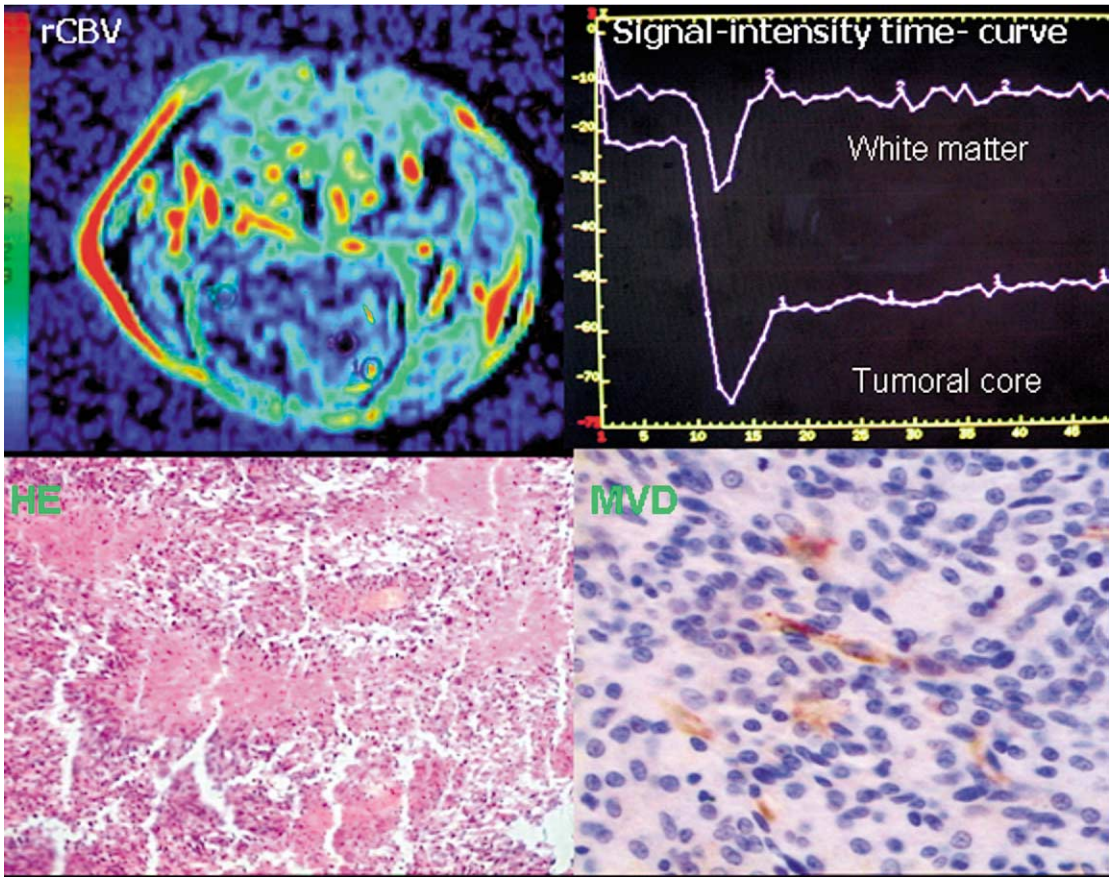

Figure 7. Perfusion-weighted magnetic resonance imaging of C6 gliomas 4 weeks after C6 cell implantation. **(a)** Relative cerebral blood volume map (rCBV). **(b)** Signal-intensity time curve. **(c)** Hematoxylin and eosin-stained image (×50). **(d)** Immunohistochemical image of CD34 (×400). Measured values of maximum rCBV in the solid portion of tumor were increased; the signal-intensity time curve fell.

rCBV maps and measurements have been shown to correlate reliably with tumor grade and histologic findings of increased tumor measurements of MVD, the current standard for assessing the degree of angiogenesis (18).

Our findings of experimental study confirm those of previous studies of humans showing a strong positive correlation between the degree of rCBV elevation and tumor stage: gradual increases in maximum rCBV values from tumoral core were demonstrated 1 week after implantation ($P < .01$). Maximum rCBV values of 1.67 ± 0.36 and 6.11 ± 0.59 in early and late stage of tumors, respectively, suggest that rCBV measurements may improve tumor grading.

Table 2
Maximum Relative rCBV in Both Tumoral and Peritumoral Areas of C6 Gliomas

Postimplantation	Cases	Solid Tumoral Region	Peritumoral Area	*P* Value
1 week	9	0.99 ± 0.14	2.88 ± 0.21	<.05
2 weeks	10	2.07 ± 0.28	2.08 ± 0.20	>.05
3 weeks	9	5.96 ± 0.45	0.98 ± 0.17	<.001
4 weeks	8	7.24 ± 0.86	0.96 ± 0.15	<.001

Data are mean ± standard deviation.

Early-stage tumors often showed low homogeneous rCBV. Instead of a traditional MRI, which can only identify breakdown of the blood-brain barrier in the form of contrast enhancement, rCBV maps can most accurately identify increase of pathologic blood supply in the presence of an either disrupted or intact blood-brain barrier (19). Meanwhile, our study also showed that elevated rCBV levels in peritumoral normal brain regions, without MVD in early stage of tumor, especially 1 week after implantation, are attributed to a generally increased overall vessel density resulting

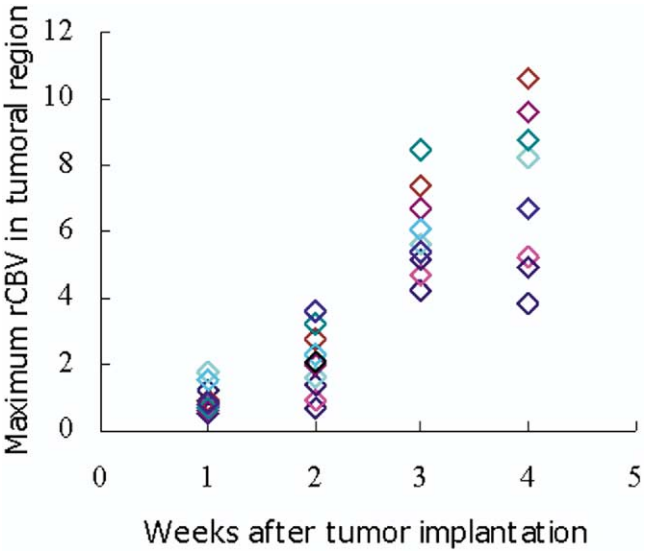

Figure 8. Measured values of maximum relative cerebral blood volume (rCBV) in the solid portion of tumor 1–4 weeks after C6 cell implantation. A statistically significant difference of maximum rCBV was present when tumors of 1 week's growth and those of 2–4 weeks' growth was compared.

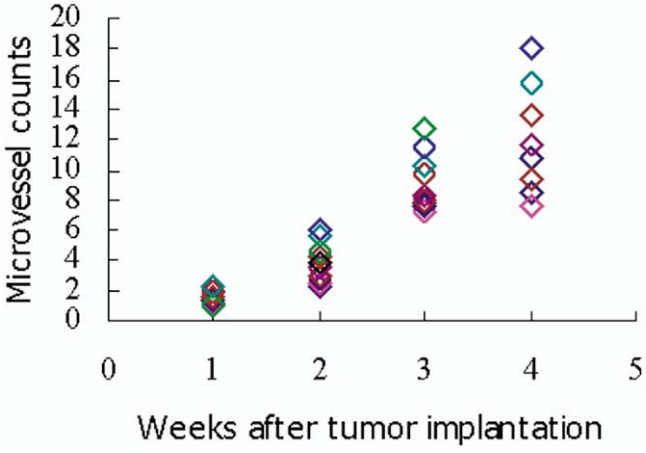

Figure 9. Measured values of microvascular density for tumors of 1–4 weeks' growth after C6 cell implantation.

from increased vessel length or tortuosity of nearby preexisting vessels without increased MVD. This shows that PWI-derived rCBV may be elevated because of expansion of the existing vascular network or formation of new capillary sprouts, or both. And the growth of tumor in an early stage may be supplied mainly by redistribution of blood flow from dilation and tortuosity of the existing vascular network of surrounding normal tissues (7). Therefore, elevation of rCBV levels in peritumoral normal brain regions may provide important

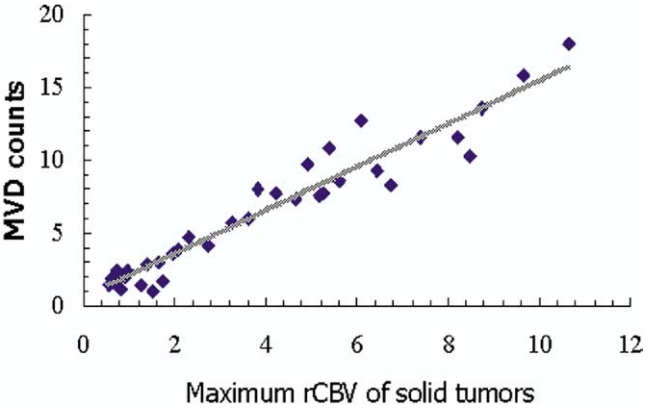

Figure 10. Maximum relative cerebral blood volume of solid C6 tumors versus microvascular density counts. There is a positive correlation between them ($P = .72$, simple regression analysis).

clue for determination of expansion of the existing vascular network in early stage of tumor.

Late-stage tumors often demonstrated significant heterogeneity and areas of high rCBV. Contrary to early-stage tumors, maximum rCBV values of late-stage tumors were significantly increased. However, there was no significant statistical difference of maximum rCBV values when tumors of 3 weeks' growth and tumors of 4 weeks' growth were compared ($P > .05$), which was slightly different from the result of MVD counting. Maximum rCBV values can reflect true regional blood volume of tumors when blood-brain barriers are intact; late-stage tumors, especially those 4 weeks after implantation, are often combined with destruction of the blood-brain barrier. The first pass of contrast material may leakage into extravascular space, and thus the produced susceptibility effects are decreased between intravascular and extravascular space near the disrupted blood-brain barrier, which is considered to cause the underestimation of the true rCBV (20). In our study, elevated rCBV levels were also present in peritumoral brain regions in late-stage tumors (ie, more than in normal white matter), which suggests increased peritumoral perfusion from tumor infiltration. In late-stage tumors, peritumoral areas demonstrate not only altered capillary morphologic findings and interstitial water, but also scattered tumor cells infiltrating along newly formed or preexisting but dilated vascular channels (17). In early-stage tumors, on the other hand, the peritumoral region contains less infiltrating tumor cells.

Although outleakage of contrast medium and expansion of the existing vascular network may affect measurement of true rCBV, our results still showed that the maximum rCBV values from tumoral core correlated well with

histologic MVD. Therefore, PWI maximum rCBV value may be a powerful tool in assessing tumor angiogenesis in vivo.

In summary, MRI rCBV of brain tumors not only is feasible, but also offers clinically relevant physiologic data not obtainable by conventional MRI. Many MRI parameters—including CBV, cerebral blood flow, mean transit time, and permeability—can, in principle, be derived by following the injection of a compact bolus of contrast media. Among them, blood vessel permeability in tumors is another such a marker that is thought to reflect the rate of angiogenesis except for CBV. However, most previous studies of blood vessel permeability in humans have typically been performed using T_1-weighted techniques (21). Permeability measurements of glial tumors using T_2-weighted dynamic susceptibility technique are still controversial and remain under investigation because of T_1-weighted effects (22). In addition, although several studies suggest that permeability is correlated well with malignancy, this suggestion does not establish a link between angiogenesis and permeability or angiogenesis and malignancy (22). Therefore, use of CBV rather than a permeability map to investigate angiogenesis of gliomas model in our study is because of the previously discussed potential limitations of permeability.

ACKNOWLEDGMENTS

The authors are grateful to Weiguo Jiang, PhD, for his expertise and assistance with microscopy and photography, and to Hong Shu and Weiliang Ma for the histologic studies.

REFERENCES

1. Johnson PC, Hunt SJ, Drayer BP. Human cerebral gliomas: correlation of postmortem MR imaging and neuropathologic findings. Radiology 1989; 170:211–217.
2. Tien RD, Felsberg GJ, Friedman H, et al. MR imaging of high-grade cerebral gliomas: value of diffusion-weighted echoplanar pulse sequences. AJR Am J Roentgenol 1994; 162:671–677.
3. Castillo M, Smith JK, Kwock L, et al. Apparent diffusion coefficients in the evaluation of high-grade cerebral gliomas. AJNR Am J Neuroradiol 2001; 22:60–64.
4. Stadnik TW, Chaskis C, Michotte A, et al. Diffusion-weighted MR imaging of intracerebral masses: comparison with conventional MR imaging and histologic findings. AJNR Am J Neuroradiol 2001; 22:969–976.
5. Aronen HJ, Gazit IE, Louis DN, et al. Cerebral blood volume maps of gliomas: comparison with tumor grade and histologic findings. Radiology 1994; 191:41–51.
6. Roberts HC, Roberts TP, Brasch RC, et al. Quantitative measurement of microvascular permeability in human brain tumors achieved using dynamic contrast-enhanced MR imaging: correlation with histologic grade. AJNR Am J Neuroradiol 2000; 21:891–899.
7. Cha S, Johnson G, Wadghiri YZ, et al. Dynamic, contrast-enhanced perfusion MRI in mouse gliomas: correlation with histopathology. Magn Reson Med 2003; 49:848–855.
8. Barth RF. Rat brain tumor models in experimental neuro-oncology: the 9L, C6, T9, F98, RG2 (D74), RT-2 and CNS-1 gliomas. J Neurooncol 1998; 36:91–102.
9. Weidner N, Barbarishi M, Gasparini G, et al. Microvascular density qualification in breast carcinoma. Applied Immunhistochem 1995; 3:75–79.
10. Grobben B, De Deyn PP, Slegers H. Rat C6 glioma as experimental model system for the study of glioblastoma growth and invasion. Cell Tissue Res 2002; 310:257–270.
11. Thorsen F, Ersland L, Nordli H, et al. Imaging of experimental rat gliomas using a clinical MR scanner. J Neurooncol 2003; 63:225–231.
12. Stadnik TW, Chaskis C, Michotte A, et al. Diffusion-weighted MR imaging of intracerebral masses: comparison with conventional MR imaging and histologic findings. AJNR Am J Neuroradiol 2001; 22:969–976.
13. Bulakbasi N, Kocaoglu M, Ors F, et al. Combination of single-voxel proton MR spectroscopy and apparent diffusion coefficient calculation in the evaluation of common brain tumors. AJNR Am J Neuroradiol 2003; 24:225–233.
14. Fan G, Sun B, Wu Z, et al. In vivo single-voxel proton MR spectroscopy in the differentiation of high-grade gliomas and solitary metastases. Clin Radiol 2004; 59:77–85.
15. Sugahara T, Korogi Y, Kochi M, et al. Usefulness of diffusion-weighted MRI with echo-planar technique in the evaluation of cellularity in gliomas. J Magn Reson Imaging 1999; 9:53–60.
16. Brunberg JA, Chenevert TL, McKeever PE, et al. In vivo MR determination of water diffusion coefficients and diffusion anisotropy: correlation with structural alternation in gliomas of the cerebral hemispheres. AJNR Am J Neuroradiol 1995; 16:361–371.
17. Bello L, Giussani C, Carrabba G, et al. Angiogenesis and invasion in gliomas. Cancer Treat Res 2004; 117:263–284.
18. Pathak AP, Schmainda KM, Ward BD, et al. MR-derived cerebral blood volume maps: issues regarding histological validation and assessment of tumor angiogenesis. Magn Reson Med 2001; 46:735–747.
19. Le Duc G, Peoc'h M, Remy C, et al. Use of T2-weighted susceptibility contrast MRI for mapping the blood volume in the glioma-bearing rat brain. Magn Reson Med 1999; 42:754–761.
20. Schmainda KM, Rand SD, Joseph AM, et al. Characterization of a first-pass gradient-echo spin-echo method to predict brain tumor grade and angiogenesis. AJNR Am J Neuroradiol 2004; 25:1524–1532.
21. Roberts HC, Roberts TPL, Brasch RC, et al. Quantitative measurement of microvascular permeability in human brain tumors achieved using dynamic contrast-enhanced MR imaging: correlation with histologic grade. AJNR Am J Neuroradiol 2000; 21:891–899.
22. Provenzale JM, Wang GR, Brenner T, et al. Comparison of permeability in high-grade and low-grade brain tumors using dynamic susceptibility contrast MR imaging. AJR Am J Roentgenol 2002; 178:711–716.